Human Molecular Genetics, 2015, 1–16

doi: 10.1093/hmg/ddv224
Original Article

ORIGINAL ARTICLE

Decreased glycogen synthase kinase-3 levels and activity contribute to Huntington's disease

Marta Fernández-Nogales[1,2], Félix Hernández[1,2], Andrés Miguez[2,3,4], Jordi Alberch[2,3,4], Silvia Ginés[2,3,4], Esther Pérez-Navarro[2,3,4] and José J. Lucas[1,2,*]

[1]Center for Molecular Biology "Severo Ochoa" (CBMSO) CSIC/UAM, 28049 Madrid, Spain, [2]Networking Research Center on Neurodegenerative Diseases (CIBERNED), Instituto de Salud Carlos III, Madrid, Spain, [3]Departament de Biologia Cellular, Immunologia i Neurociències, Facultat de Medicina, Universitat de Barcelona, 08036 Barcelona, Spain and [4]Institut d'Investigacions Biomèdiques August Pi i Sunyer (IDIBAPS), 08036 Barcelona, Spain

*To whom correspondence should be addressed at: Centro de Biología Molecular "Severo Ochoa" (CSIC/UAM), C/ Nicolás Cabrera, 1, Campus UAM de Cantoblanco, 28049 Madrid, Spain. Tel: +34 91 196 4552/+34 91 196 4582; Email: jjlucas@cbm.csic.es

Abstract

Huntington's disease (HD) is a hereditary neurodegenerative disorder characterized by brain atrophy particularly in striatum leading to personality changes, chorea and dementia. Glycogen synthase kinase-3 (GSK-3) is a serine/threonine kinase in the crossroad of many signaling pathways that is highly pleiotropic as it phosphorylates more than hundred substrates including structural, metabolic, and signaling proteins. Increased GSK-3 activity is believed to contribute to the pathogenesis of neurodegenerative diseases like Alzheimer's disease and GSK-3 inhibitors have been postulated as therapeutic agents for neurodegeneration. Regarding HD, GSK-3 inhibitors have shown beneficial effects in cell and invertebrate animal models but no evident efficacy in mouse models. Intriguingly, those studies were performed without interrogating GSK-3 level and activity in HD brain. Here we aim to explore the level and also the enzymatic activity of GSK-3 in the striatum and other less affected brain regions of HD patients and of the R6/1 mouse model to then elucidate the possible contribution of its alteration to HD pathogenesis by genetic manipulation in mice. We report a dramatic decrease in GSK-3 levels and activity in striatum and cortex of HD patients with similar results in the mouse model. Correction of the GSK-3 deficit in HD mice, by combining with transgenic mice with conditional GSK-3 expression, resulted in amelioration of their brain atrophy and behavioral motor and learning deficits. Thus, our results demonstrate that decreased brain GSK-3 contributes to HD neurological phenotype and open new therapeutic opportunities based on increasing GSK-3 activity or attenuating the harmful consequences of its decrease.

Introduction

Huntington's disease (HD) is an inherited neurodegenerative disorder characterized by motor, psychiatric and cognitive symptoms (1). The major site of neuronal loss is the striatum although brain atrophy extents to other regions (1). HD is caused by a CAG triplet expansion in exon 1 of the huntingtin (htt) gene (2) leading to an expanded polyglutamine stretch in the mutant protein. The exact mechanism by which expanded CAG mRNA sequence and/or polyglutamine-induced neurodegeneration remains unknown. However, N-terminal forms of mutant huntingtin (mhtt) are known to accumulate in the cytoplasm and interact with several proteins causing impairment of signaling pathways (3).

Glycogen synthase kinase-3 (GSK-3) is a serine/threonine kinase expressed in all tissues, although levels are more abundant in the brain. There are two paralogs of this enzyme, GSK-3α and GSK-3β, which are almost identical, particularly in their catalytic domains (4), and that are regulated by multiple mechanisms (5–7) including substrate priming, cellular trafficking, incorporation into protein complexes like axin/APC, D2R/β-arrestin (8,9) or

Received: May 28, 2015. **Revised:** May 28, 2015. **Accepted:** June 11, 2015

D2R/Disc1 (10) and post-translational modifications such as phosphorylation at an N-terminal serine residue (Ser 21/9 for α and β, respectively) that renders the kinase inactive in some of its possible functional scenarios (5). GSK-3 is a pleiotropic enzyme as it is able to phosphorylate more than hundred proteins involved in functions such as metabolism, cell structure, gene expression including epigenetics, and apoptosis (5,6).

GSK-3 activity is tuned by self-activating mechanisms (5) and it has been postulated that abnormally increased GSK-3 activity contributes to the pathogenesis of neurodegenerative and psychiatric diseases like Alzheimer's disease (6,11) and bipolar disorder (12,13). Accordingly, the non-selective GSK-3 inhibitor lithium is used as a therapy for bipolar disorder (14) and has been explored in clinical trials for Alzheimer's disease (15,16), and selective GSK-3 inhibitors are under development for possible therapeutic interventions (5,17–19).

Regarding HD, GSK-3 inhibition has been shown to protect against polyglutamine-induced cell death and to reduce the number of huntingtin inclusions in cell (20,21) and invertebrate animal (22,23) models. However, therapeutic efficacy of GSK-3 inhibition was not evident in rodent models (24) as GSK-3 inhibitors showed beneficial effects only when combined with other drugs (25,26) particularly those that stimulate autophagy, which may counteract the decreased autophagy elicited by GSK-3 inhibition (27). However, the main reason for GSK-3 inhibitors not showing a clear beneficial effect by themselves in HD mouse models could be that GSK-3 levels and activity might not be increased in HD. In fact, we and others have previously found increased N-terminal serine phosphorylation of GSK-3 in striatum and other brain regions of various HD mouse models thus suggesting that GSK-3 activity, rather than increased, might be reduced in HD (28–30) and, although no data are available regarding striatum of postmortem human HD brain, decreased GSK-3β levels have recently been reported in frontal cortex of HD brains (29). In line with the notion that decreased striatal GSK-3 activity could contribute to HD, transgenic mice with forebrain expression of a dominant-negative form of GSK-3 show reduced GSK-3 activity and increased neuronal apoptosis in the striatum and also motor deficits in striatal-dependent tasks, thus showing an HD-like phenotype (31,32).

In the present study, we aim to explore the level and also the enzymatic activity of GSK-3 in the striatum and other affected brain regions of HD patients and mouse models to then elucidate the possible contribution of its alteration to HD pathogenesis by genetic manipulation in mice.

Results

Decreased GSK-3 level and activity in HD brain

To investigate the status of GSK-3 in the brain of HD patients, here we analyzed for the first time the level of GSK-3 in striatum of HD patients and non-affected individuals. By western blot, we observed that levels of both GSK-3 isoforms were dramatically decreased in the striatum of HD brains respect to control brains ($P = 0.028$ for α and $P = 0.045$ for β). We also analyzed samples from cortex and hippocampus and a decrease of both isoforms was also observed in cortex ($P = 0.006$ for α and $P = 0.01$ for β) while only a tendency to decrease was observed in hippocampus (Fig. 1A). As shown in Supplementary Material, Figure S1A–C, no obvious contribution of sex, age or postmortem interval (PMI) is observed to these effects. Interestingly, these decreases in GSK-3α and GSK-3β protein levels in striatum and cortex of HD brains do not seem to be due to altered transcription of the GSK-3α and β genes as quantitative RT-PCR analysis of RNA extracted from HD brains revealed that the transcripts of GSK-3α or β are not diminished in the HD samples (Fig. 1B).

As a way to explore whether the observed decrease in GSK-3 protein levels would precede neurodegeneration rather than reflecting a late consequence of the neuronal loss dysfunction, we analyzed the samples with low Vonsattel grade separately. As shown in Supplementary Material, Figure S1D, in this limited number of low-grade HD postmortem brains (Grade 1, $n = 1$; Grade 2, $n = 3$), the striatal decrease seems to happen even in the Grade 1 case and the cortical decrease seems to manifest from Grade 2 onwards. This suggests that the observed decrease might predate neurodegeneration rather than just being consequence of the neurodegeneration of the vulnerable cells and preservation of the speared ones.

GSK-3 protein levels are not a direct indicator of GSK-3 activity and, as mentioned, an indirect way to explore GSK-3 activity in some of its possible functional scenarios is by analyzing the levels of phosphorylation of GSK-3 at serine-9 for GSK-3β and at serine-21 for GSK-3α. We thus performed western blot analysis of the inhibitory N-terminal serine phosphorylation of GSK-3 in control and HD samples. However, the previously reported (33) instability of the epitope in human brain tissue associated with postmortem interval, precluded conclusive results. Then, as a direct indicator of activity, we performed an *in vitro* GSK-3 enzymatic activity assay on homogenates from striatum, cortex and hippocampus of HD patients and controls using a pre-phosphorylated peptide as a well-characterized substrate of GSK-3. In line with the observed decrease in GSK-3 protein levels, we detected a significant decrease in GSK-3 activity in the striatum (73.9%; $P = 0.005$) and cortex (56.5%; $P = 0.001$) of HD cases versus controls while only a tendency was observed in hippocampus (Fig. 1C). These results indicate that GSK-3 protein levels and activity are decreased in the two most affected brain regions of HD patients.

Decreased GSK-3 levels and activity in the R6/1 mouse model of HD

We and others have previously found increased N-terminal serine phosphorylation of GSK-3 as indicator of reduced GSK-3 activity in selected regions of R6/1 mouse model of HD (28,29). To further explore if the results obtained from human HD brain can be recapitulated in this mouse model, we analyzed GSK-3 levels, p-Ser-GSK-3 levels and activity in the striatum, cortex and hippocampus of R6/1 mice at pre-symptomatic ages (4 and 8 weeks), at an early symptomatic age (3.5 months) and at a late symptomatic age (7.5 months). Analysis of GSK-3 protein levels by western blot showed a tendency to decreased GSK-3 level in cortex of 8-week-old R6/1 mice respect WT mice (data not shown) and the earliest significant decreases were found in striatum ($P < 0.0001$) and cortex ($P = 0.006$) of early symptomatic (3.5 months) R6/1 mice compared with WT animals (Fig. 2A and B). Regarding the hippocampus, a significant decrease in GSK-3 level is found only at late symptomatic stages of the R6/1 mice (Fig. 2B). As observed in the brain of HD patients, this decrease was not a consequence of diminished transcript levels as qRT-PCR analysis revealed that transcript level of GSK-3α and β genes is not significantly altered (Fig. 2C).

As mentioned, an indirect way to explore GSK-3 activity in some of its possible functional scenarios is by analyzing the levels of phosphorylation at the N-terminal serine residues. In good agreement with previous reports (28,29), we observed a significant increase in the levels of p-GSK-3 in: striatum ($P = 0.013$) of

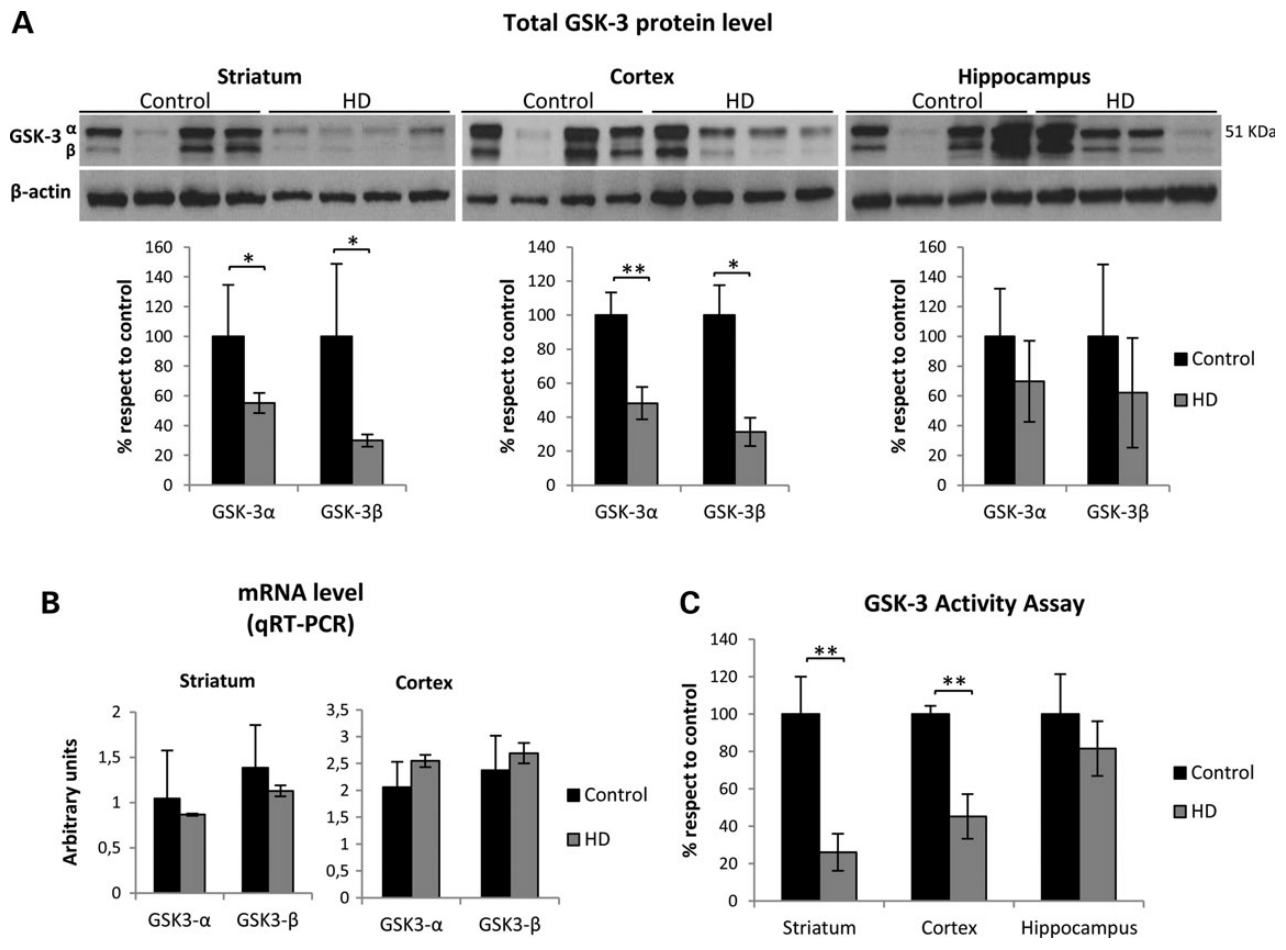

Figure 1. Analysis GSK-3 levels and activity in striatum, cortex and hippocampus of HD patients. (**A**) Western blot detection of GSK-3α/β levels in homogenates from the striatum, cortex and hippocampus of HD patients and controls ($n = 8$ for striatum, $n = 11$–10 for cortex and $n = 4$ for hippocampus; Student's *t*-test, $^{**}P < 0.01$, $^{*}P < 0.05$). (**B**) Quantitative RT-PCR analysis of GSK-3α and GSK-3β mRNA in striatum and cortex of HD and control samples ($n = 5$–7 for striatum and $n = 9$-8 for cortex; only samples with RNA integrity number (RIN) >5 were included in the analysis). (**C**) *In vitro* GSK-3 activity assay performed in homogenates from the striatum, cortex and hippocampus of HD patients and control subjects ($n = 8$ for striatum, $n = 10$ for cortex and $n = 3$–9 for hippocampus, Student's *t*-test; $^{**}P < 0.01$, $^{*}P < 0.05$).

presymtomatic (8 weeks old) R6/1 mice (data not shown); in striatum ($P = 0.049$), cortex ($P = 0.005$) and hippocampus ($P = 0.00025$) of 3.5-month-old early symptomatic R6/1 mice (Fig. 2D); and in striatum ($P = 0.019$), cortex ($P = 0.002$) and hippocampus ($P = 0.009$) of 7.5-month-old late symptomatic R6/1 mice compared with WT mice (Fig. 2E). These findings were confirmed by immunohistochemistry in striatum and cortex of 3.5-month-old R6/1 mice that show a significant increase in the number of p-Ser-GSK-3α/β-positive cells (Supplementary Material, Fig. S2A) and double immunofluorescence with astrocytic (GFAP) or neuronal (NeuN) markers (Supplementary Material, Fig. S2B and C) revealed that the cells with increased p-Ser-GSK-3α/β staining are neurons. Together, the data with the anti-p-Ser-GSK-3α/β antibody further suggest decreased GSK-3 activity in the brain of R6/1 mice.

To confirm that decreased total levels and increased p-GSK-3 indeed result in decreased activity, we performed the GSK-3 enzymatic activity assay on homogenates from striatum, cortex and hippocampus of R6/1 mice. The earliest significant decrease in GSK-3 activity was observed in striatum (23%; $P = 0.002$) of early symptomatic (3.5 months old) R6/1 mice (Fig. 2H) compared with WT and similar results (21.6%; $P = 0.006$) were observed in late symptomatic (7.5 months old) R6/1 mice (Fig. 2I). A tendency to decrease was also observed in cortex and hippocampus of 7.5-month-old R6/1 mice (Fig. 2I). To try to explain why the decrease in activity assay is restricted to the striatum, we decided to analyze also phosphorylation of GSK-3 at the Tyr216/279 residues which is believed to correlate with activated GSK-3 (5). As shown in Supplementary Material, Figure S3, p-Tyr279-GSK-3α and p-Tyr216GSK-3β are significantly decreased only in striatum ($P = 0.004$ for α and $P = 0.028$ for β) of R6/1 mice while they are significantly increased in cortex ($P = 0.015$ for α and $P = 0.025$ for β) and hippocampus ($P = 0.015$ for α and $P = 0.012$ for β) of R6/1 mice. This may be the reason why the decrease in enzymatic activity assay only reaches significance in striatum.

Generation of R6/1 mice with varying levels of transgenic GSK-3

To test whether the observed decreased GSK-3 level and activity in the brain of R6/1 mice contributes to their HD-like phenotype, we decided to explore the consequences of modifying GSK-3 levels by genetic manipulation. For this, we produced R6/1 mice with varying levels of transgenic GSK-3 expression. We have previously generated the BitetO-β-Gal/GSK-3β transgenic mouse line (34) that harbors a DNA construct with a GSK-3β sequence and, as a reporter of gene expression, also a β-galactosidase sequence with a nuclear localization signal. These two coding sequences are under the control of the two CMV minimal promoters

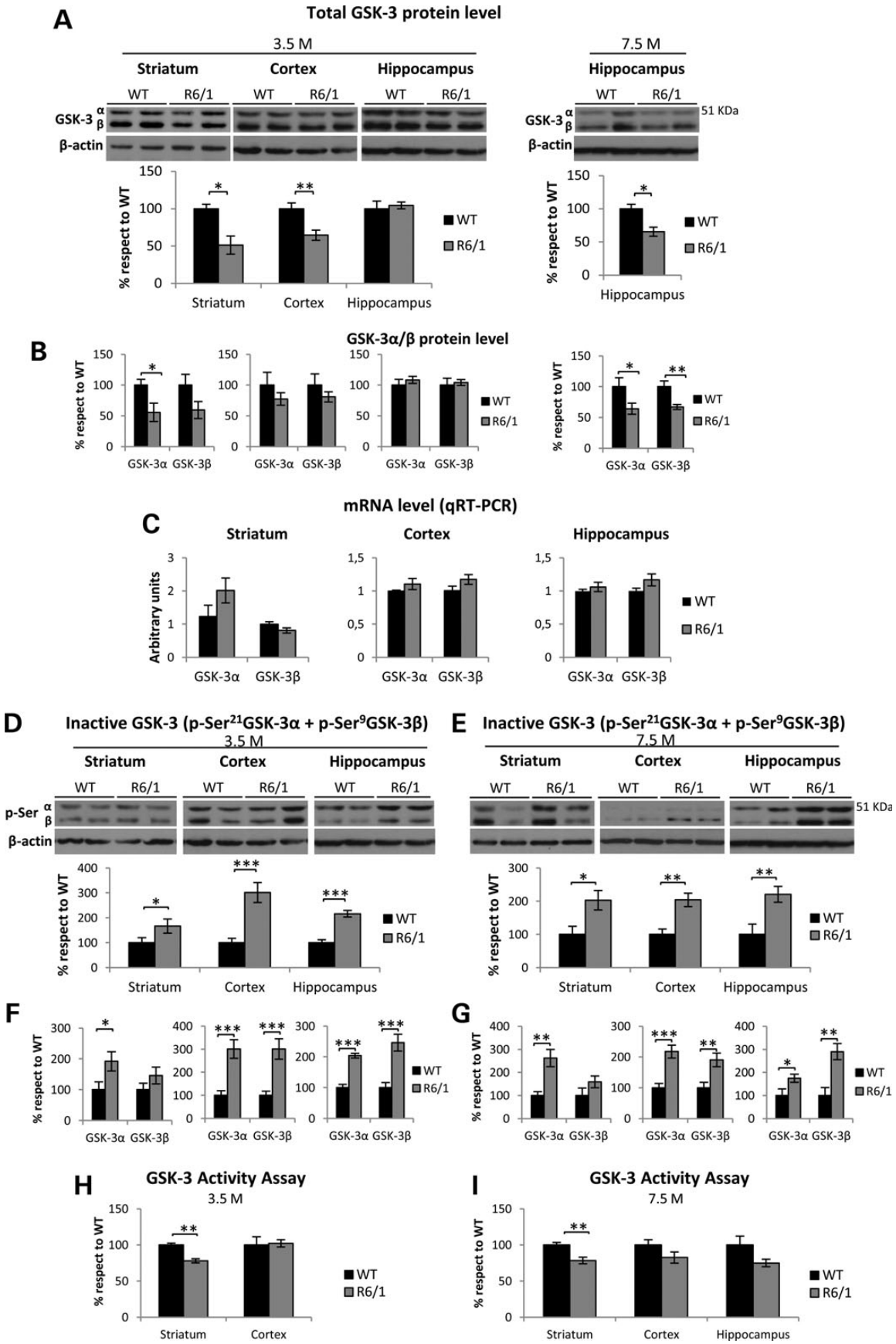
A
Total GSK-3 protein level
3.5 M
7.5 M
Striatum
Cortex
Hippocampus
WT
R6/1
GSK-3 α β
β-actin
51 KDa
% respect to WT
B
GSK-3α/β protein level
GSK-3α
GSK-3β
C
mRNA level (qRT-PCR)
Arbitrary units
D
Inactive GSK-3 (p-Ser21GSK-3α + p-Ser9GSK-3β)
p-Ser α β
E
F
G
H
GSK-3 Activity Assay
I

(CMVmin) in the bidirectional tetO promoter (BitetO) (Fig. 3A). These BitetO-β-Gal/GSK-3β mice show a modest expression of the β-Gal reporter in brain areas such as the striatum, cortex or hippocampus (Fig. 3B) and of transgenic GSK-3β mRNA (Fig. 3F) and only those cells with high levels of the reporter β-Gal show increased GSK-3 levels as evidenced by double β-Gal/GSK-3 immunofluorescence (Fig. 3C). In previous characterizations of these mice, no obvious behavioral phenotypes have been observed (35,36). Here, we will refer to these animals as LowTgGSK-3 mice. Besides, we have also previously reported that when LowTgGSK-3 mice are combined with mice expressing the tetracycline transactivator (tTA, also known as Tet-Off) under control of the forebrain neuronal promoter CamKII (CamKII-tTA mice), the resulting double transgenic mice CamKII-tTA + BitetO-β-Gal/GSK-3β (Fig. 3D) show robust neuronal expression in all forebrain regions such as the striatum, cortex and hippocampus (Fig. 3E and F). We will refer to these mice as HighTgGSK-3 mice. These mice have been reported to show increased neuronal cell death, particularly in the hippocampus, and to display Alzheimer's disease-like biochemical and behavioral alterations (34–36). In summary, the use of this conditional transgenic mouse system enables the generation of mice with low or high level of GSK-3 transgenic expression.

To generate R6/1 mice with varying levels of transgenic GSK-3 overexpression, we followed the breeding protocol shown in Figure 3G to set HighTgGSK-3 × R6/1 crossing that renders the six experimental genotypes relevant for this study: wild-type (WT), LowTgGSK-3, HighTgGSK-3, R6/1, R6/1 + LowTgGSK-3 and R6/1 + HighTgGSK-3 mice. A total of 270 mice were generated (Fig. 3G) that were distributed among the experimental genotypes as follows: WT ($n = 53$), LowTgGSK-3 ($n = 68$), HighTgGSK-3 ($n = 47$), R6/1 ($n = 46$), R6/1 + LowTgGSK-3 ($n = 39$) and R6/1 + HighTgGSK-3 ($n = 17$). They do not follow a Mendelian segregation of genotypes (χ^2 analysis $P = 0$) as the percentage of R6/1+HighTgGSK-3 mice (5.1%) was lower than expected (12.5%) thus indicating that there is embryonic or perinatal lethality due to the combination of toxicities associated to mhtt and excess of GSK-3 expression in R6/1+HighTgGSK-3 mice.

We then verified by western blot that the decreased GSK-3 levels in striatum of R6/1 mice are progressively corrected by the low- and high-expression transgenes (Fig. 3H). A similar effect was observed in the enzymatic activity assay in which the low- and high-expression transgenes counteract the significant decrease observed in the striatum of R6/1 mice respect to WT mice (Fig. 3I).

Low transgenic overexpression of GSK-3 attenuates brain atrophy in R6/1 mice

As a global indicator of whether modest or high transgenic expression of GSK-3 would have a positive effect on the progression of the HD phenotype in R6/1 mice, analysis of striatal, cortical and hippocampal volume was performed in sagittal sections obtained from 8-month-old WT, R6/1, R6/1 + LowTgGSK-3 and R6/1 + HighTgGSK-3 mice by using the Cavalieri method (Fig. 4A and B). As extensively reported, R6/1 mice presented a reduction in the volume of these brain regions compared with WT mice but, interestingly, R6/1 + LowTgGSK-3 mice showed attenuated atrophy as the volume of cortex ($P = 0.0163$) and hippocampus ($P = 0.0252$) was higher compared with R6/1 mice and a tendency was also observed in the striatum (Fig. 4A and B). In contrast, no differences were observed between R6/1 and R6/1 + HighTgGSK-3 mice thus indicating that modest GSK-3 overexpression to correct the inherent decrease in R6/1 mice is beneficial but that excessive GSK-3 production is no longer beneficial probably due to the well-documented neuronal toxicity of excessive GSK-3 activity (34,37).

We also analyzed the effect of transgenic GSK-3 expression on the load of Htt-positive aggregates in R6/1 mice. The number and size of aggregates were analyzed in striatum of 8-month-old R6/1, R6/1 + LowTgGSK-3 and R6/1 + HighTgGSK-3 mice by immunostaining with an anti-N-terminal-Htt antibody. We found no changes in the number of striatal inclusions in R6/1 + LowTgGSK-3 and R6/1 + HighTgGSK-3 mice when compared with R6/1 mice (Fig. 4C and D). However, there is a tendency to increase the size of the inclusions proportional to the increase in the expression of TgGSK-3 becoming significant in R6/1 + HighTgGSK-3 mice compared with R6/1 mice (Fig. 4D, $P = 0.035$).

Low transgenic overexpression of GSK-3 attenuates motor and cognitive deficits in R6/1 mice

We then assessed whether transgenic GSK-3 expression, particularly the moderate one that was able to correct the brain atrophy in R6/1 mice, would also attenuate the motor and cognitive HD-like phenotype of these mice. For this, we first analyzed mice of the six experimental genotypes in the open-field test automated activity cages and found that the hypoactivity observed in R6/1 mice respect to WT mice at 4.5 months of age, as evidenced by a decrease in ambulatory distance and vertical counts, was improved in R6/1+LowTgGSK-3 and R6/1+HighTgGSK-3 mice during the exploratory time (0–5 min) but interestingly only R6/1 +lowTgGSK-3 mice showed improved performance during the 5–15 min test time (Fig. 5A and B). Similar results were obtained when male and female mice were analyzed separately (Supplementary Material, Fig. S4).

The effect of the GSK-3 transgenes was similar in the accelerating rotarod test. Mice were analyzed at 2, 4, 6 and 8 months of age on the accelerating rotarod (from 4 to 40 rpm) during a 5-min period, in four trials with 1 h inter-trial periods. As expected, all mice expressing mhtt showed a deficit in this motor coordination task from 4 months of age that progressively worsens until the late symptomatic age of 8 months (data not shown). Interestingly, when analyzing the latency to fall as a percentage respect to R6/1 mice, R6/1 + LowTgGSK-3 mice performed significantly

Figure 2. Analysis of GSK-3 levels and activity in the striatum, cortex and hippocampus of R6/1 mice. (**A**) Western blot detection of total GSK-3 levels in homogenates from the striatum, cortex and hippocampus of 3.5-month-old R6/1 and WT mice and from hippocampus of 7.5-month-old R6/1 and WT mice ($n = 7$–6 for striatum, $n = 7$–6 for cortex and $n = 7$ for hippocampus at 3.5 months old and $n = 6$–7 for hippocampus of mice at 7.5 months old; Student's *t*-test; $^*P < 0.05$, $^{**}P < 0.01$). (**B**) Quantification of GSK-3α and β levels in A (Student's *t*-test; $^*P < 0.05$, $^{**}P < 0.01$). (**C**) Quantitative RT-PCR analysis of GSK-3α and GSK-3β mRNA in striatum, cortex and hippocampus of 9-month-old R6/1 mice ($n = 5$). (**D**) Western blot detection of total p-Ser-GSK-3 levels in homogenates from striatum, cortex and hippocampus of R6/1 and WT mice at 3.5 months of age ($n = 7$ for striatum, $n = 7$ for cortex and $n = 7$ for hippocampus; Student's *t*-test; $^{**}P < 0.01$, $^*P < 0.05$). (**E**) Western blot detection of total p-Ser-GSK-3 levels in homogenates from striatum, cortex and hippocampus of 7.5-month-old R6/1 and WT mice ($n = 7$ for striatum, $n = 7$ for cortex and $n = 7$ for hippocampus; Student's *t*-test; $^{**}P < 0.01$, $^*P < 0.05$). (**F**) Quantification of p-Ser-GSK-3α and β levels in D (Student's *t*-test; $^{***}P < 0.001$, $^*P < 0.05$). (**G**) Quantification of p-Ser-GSK-3α/β levels in (E); (Student's *t*-test; $^{***}P < 0.001$, $^{**}P < 0.01$, $^*P < 0.05$). (**H** and **I**) *In vitro* GSK-3 activity assay performed in homogenates of the striatum and cortex ($n = 5$–7 for striatum and $n = 6$ for cortex; Student's *t*-test; $^{**}P < 0.01$) from R6/1 and WT mice at 3.5 months of age (H) and in striatum, cortex and hippocampus at 7.5 months of age (I) ($n = 5$–6 for striatum, $n = 6$–5 for cortex and $n = 5$ for hippocampus, Student's *t*-test; $^{**}P < 0.01$).

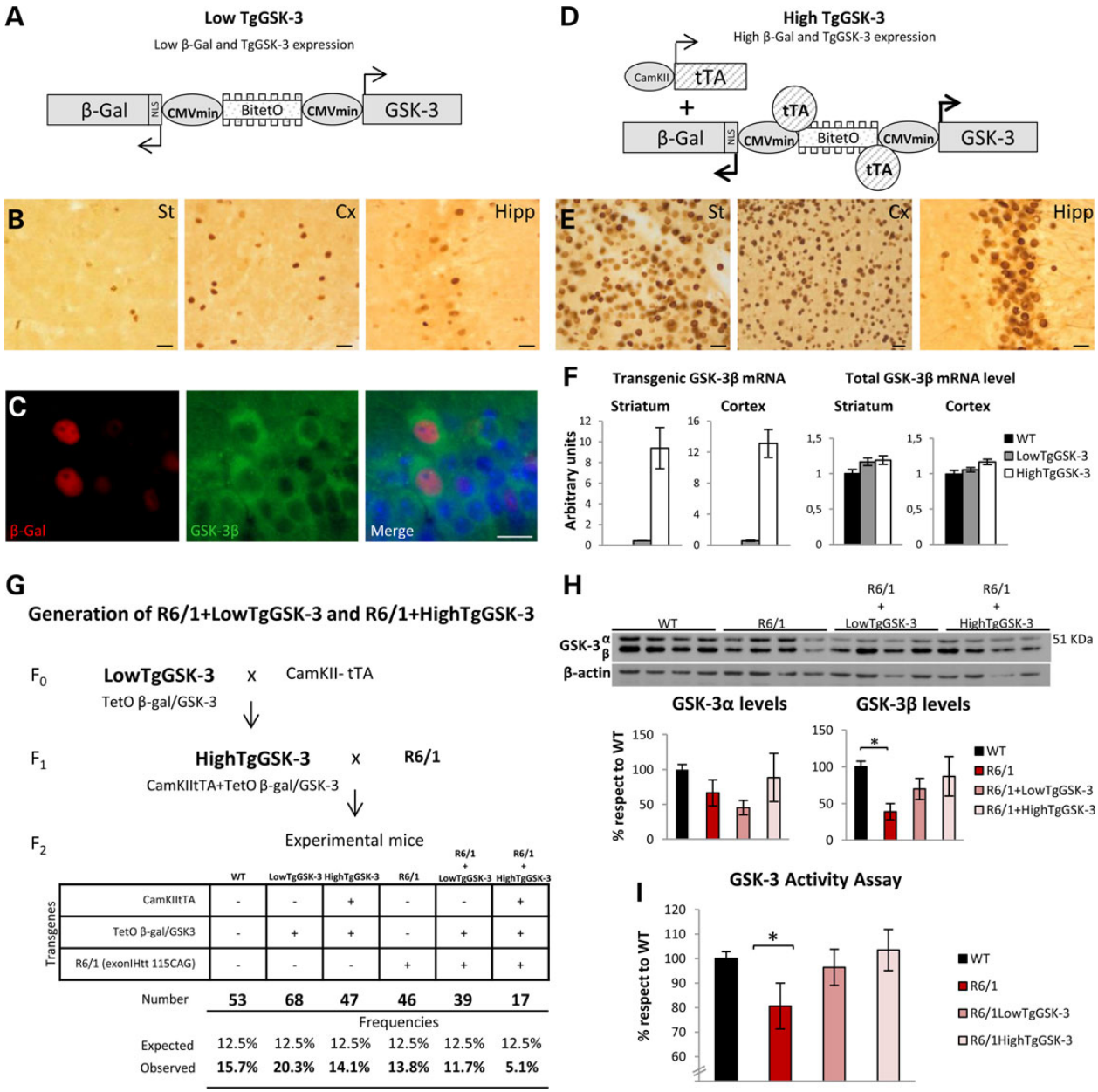

Figure 3. Generation of R6/1 mice with varying levels of transgenic GSK-3 expression. (**A**) Diagram showing the structure of the GSK-3 construct used for transgenesis in LowTgGSK-3. The bidirectional Bi-tetO promoter is followed in one direction by the GSK-3 cDNA sequence, and by the β-galactosidase (β-Gal) sequence with a nuclear localization signal (NLS) in the other direction. (**B**) β-Gal immunohistochemistry on sagittal brain sections from 8-month-old LowTgGSK-3 mice in striatum, cortex and hippocampus. Scale bar corresponds to 20 μm. (**C**) Double immunofluorescence of β-gal (red) and GSK-3β (green) in hippocampal sections from LowTgGSK-3 mice. Scale bar corresponds to 20 μm. (**D**) Schematic representation of the generation of HighTgGSK-3 mice. (**E**) β-Gal immunohistochemistry on sagittal brain sections from 8-month-old WT, LowTgGSK-3 and HighTgGSK-3 mice in striatum, cortex and hippocampus. Scale bar corresponds to 20 μm. (**F**) RT-PCR analysis of transgenic GSK-3β mRNA and total GSK-3β mRNA in striatum and cortex of LowTgGSK-3 and HighTgGSK-3 respect to WT. (**G**) Schematic representation of the breeding protocol to obtain R6/1 mice with LowTgGSK-3 or HighTgGSK-3. Number of mice of each of the six experimental genotypes obtained for the whole study is shown as well as the observed and the expected frequencies. (**H**) Western blot detection of GSK-3α/β in homogenates from striatum of WT, R6/1, R6/1 + LowTgGSK-3 and R6/1 + HighTgGSK-3 mice ($n = 4$; ANOVA, followed by Games–Howell *post hoc* test; $^*P < 0.05$). (**I**) *In vitro* GSK-3 activity assay performed on homogenates of the striatum from WT ($n = 12$), R6/1 ($n = 13$), R6/1 + LowTgGSK-3 ($n = 5$) and R6/1 + HighTgGSK-3 ($n = 6$) mice at 3.5 months of age (ANOVA, followed by Games–Howell *post hoc* test; $^*P < 0.05$).

better than R6/1 and R6/1 + HighTgGSK-3 mice at 2, 4 and 6 months of age (Fig. 5C). Similar results were obtained when male and female mice were analyzed separately (Supplementary Material, Fig. S4).

Finally, we evaluated memory tasks in the six experimental genotypes in the fear conditioning test. More precisely, we performed the context dependent fear conditioning that assesses hippocampal-dependent learning and memory. Figure 5D shows representative plots of freezing/activity of mice of the six experimental genotypes, in green the percentage of time that the mouse spent freezing compared with the percentage of time that the mouse was moving (yellow). As shown in Figure 5E, R6/1 mice show a clear deficit as their percentage of time freezing is dramatically lower when compared with WT. This is most evident in males as it reaches significance for males only and for males + females together but it only shows a tendency for females

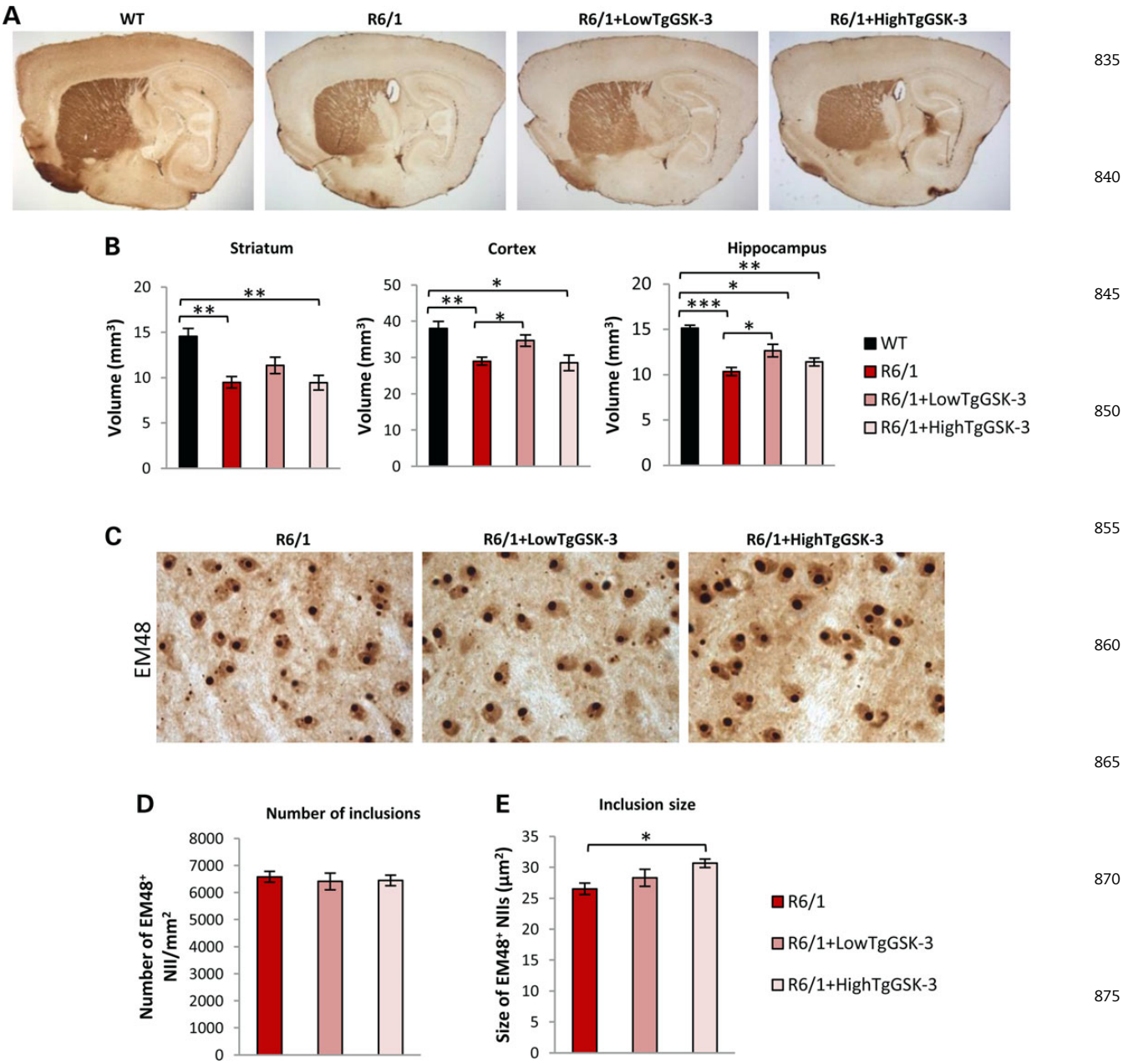

Figure 4. Forebrain volumetric analysis of R6/1 mice with varying levels of transgenic GSK-3 expression. (**A**) Representative images of DARPP-32-stained sagittal sections from WT, R6/1, R6/1 + LowTgGSK-3 and R6/1 + HighTgGSK-3 mice at 8 months of age. (**B**) The histogram shows the quantification of striatal, cortical and hippocampal volume. Results are expressed as the mean ± SEM. At least four animals per genotype were analyzed. (**C–E**) EM48 immunohistochemistry to detect striatal mhtt inclusions. (C) Images showing EM48-positive inclusions in R6/1, R6/1 + LowTgGSK-3 and R6/1 + HighTgGSK-3 mice. (D and E) Histograms showing the number (D) and size (E) of neuronal intranuclear inclusions (NIIs) in R6/1, R6/1 + LowTgGSK-3 and R6/1 + HighTgGSK-3 mice. (ANOVA, followed by DMS multiple comparisons test; *$P < 0.05$).

(Supplementary Material, Fig. S4). Interestingly, this deficit was attenuated in R6/1 + LowTgGSK-3 mice as they spent significantly more time freezing than R6/1 mice. In summary, these results demonstrate that a moderate increase in GSK-3 expression is able to attenuate both motor and cognitive deficits in R6/1 mice.

Discussion

Here we analyze for the first time in HD postmortem brain the level and activity of GSK-3 in striatum, the most affected region in this disease, and we also analyzed other affected brain regions like cortex and hippocampus. We found a dramatic decrease in GSK-3 level and activity in striatum and cortex of HD patients and similar results were obtained in the R6/1 mouse model. By combining R6/1 mice with our previously generated transgenic mouse model with conditional overexpression of GSK-3, we are able to demonstrate that the mentioned decrease in GSK-3 does contribute to HD phenotype as the brain atrophy, the locomotor hypoactivity and the deficits in motor coordination and learning of R6/1 mice are attenuated by a moderate expression of transgenic GSK-3.

The first study of GSK-3 in relation to mhtt toxicity was performed in cellular models expressing the Htt exon 1 fragment with 74 glutamines (Q74-Htt) (20). The non-selective GSK-3 inhibitor lithium, the selective inhibitor SB216763 and the

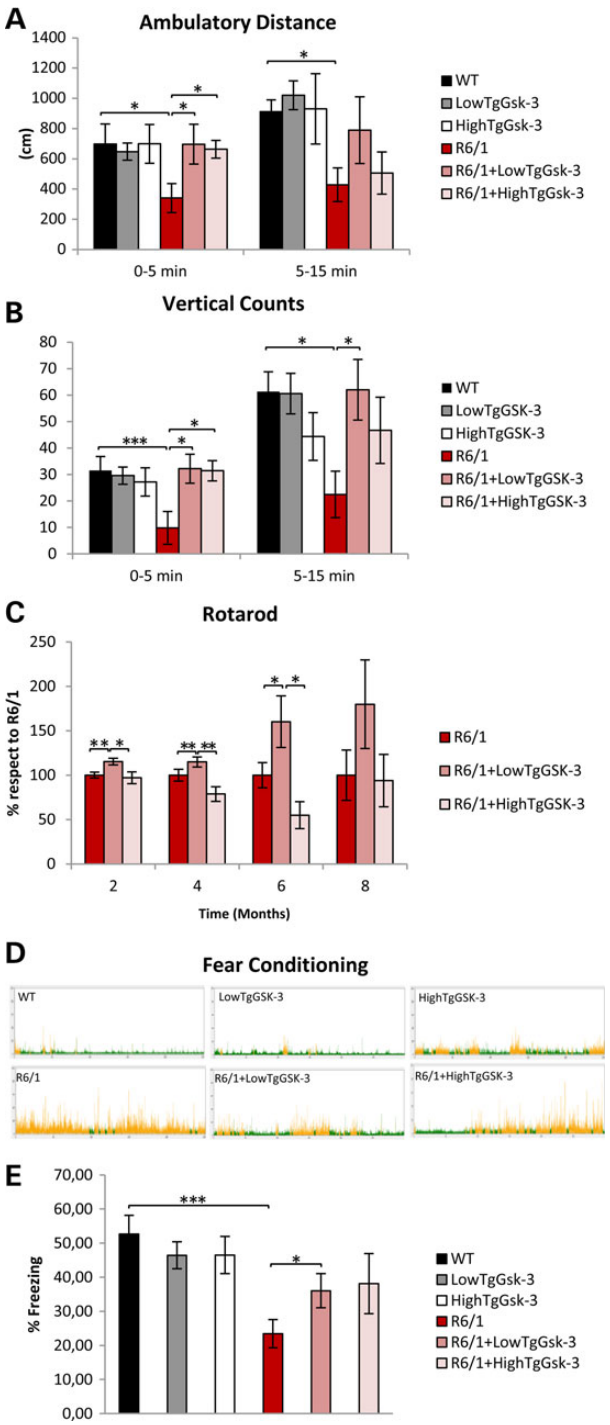

Figure 5. LowTgGSK-3 expression improves motor tasks and memory tasks in R6/1 mice. (**A** and **B**) Open-field test of WT ($n = 19$); LowTgGSK-3 ($n = 22$); HighTgGSK-3 ($n = 13$); R6/1 ($n = 19$); R6/1 + LowTgGSK-3 ($n = 17$); and R6/1 + HighTgGSK-3 ($n = 7$) mice at 4.5 months of age (Kruskal–Wallis, followed by Mann–Whitney *U*-test; $^{*}P < 0.05$, $^{***}P < 0.001$). (**C**) Rotarod. Evolution of the mean latency to fall from a rod of mice from 2 to 8 months of age. WT ($n = 25$); LowTgGSK-3 ($n = 52$); HighTgGSK-3 ($n = 28$); R6/1 ($n = 30$); R6/1 + LowTgGSK-3 ($n = 27$) and R6/1 + HighTgGSK-3 ($n = 12$) mice. The histogram shows the percentage respect to R6/1 of the latency to fall of the R6/1 + LowTgGSK-3 and R6/1 + HighTgGSK-3 mice (Kruskall Wallis, followed by Mann–Whitney *U*-test; $^{**}P < 0.01$, $^{*}P < 0.05$). (**D** and **E**) Fear conditioning-contextual test. (D) Representation of the time that the mice spent freezing (green) or not (yellow) in fear conditioning test. (E) The histogram shows the percentage of freezing in the fear conditioning-contextual test of WT ($n = 32$); LowTgGSK-3 ($n = 32$); HighTgGSK-3 ($n = 22$); R6/1 ($n = 27$); R6/1 + LowTgGSK-3 ($n = 26$) and R6/1 + HighTgGSK-3 ($n = 10$) mice at 5 months (Kruskall–Wallis, followed by Mann–Whitney *U*-test; $^{***}P < 0.001$, $^{*}P < 0.05$).

overexpression of a dominant-negative GSK-3 plasmid significantly attenuated Q74-Htt induced cell death. At that time and later, increased GSK-3 levels/activity was reported in Alzheimer's disease (6,38–42) and transgenic GSK-3 overexpression in mice had been shown to cause neurodegeneration (34,35). Accordingly, GSK-3 inhibitors were postulated to be neuroprotective in multiple cellular and animal models of neurodegeneration (17,43–45). Similarly, treatment with lithium, alone (22–24,46,47) or in combination with valproate (25), or with the selective inhibitor AR-A014418 (22) were neuroprotective in invertebrate and rodent models of HD and of other polyglutamine disorders. In the experiments in which only lithium was administered, with the exception of the R6/2 mice (24) that did not a show a clear improvement, the chemical rat model of HD (46) and the transgenic SCA1 mouse model (47) showed an improvement on motor coordination and cognition. Besides, the invertebrate models also showed attenuated PolyQ-induced cell death (22,23). However, all these studies were performed without interrogating whether GSK-3 levels or activity were increased as a consequence of PolyQ expression.

As mentioned, lithium is a non-selective GSK-3 inhibitor as it inhibits many other enzymatic activities such as inositol monophosphatase or histone deacetylase 1 (HDAC1) (48,49). Besides, lithium by itself or in combination with other compounds like rapamycin (27) and valproate (25) was found to enhance autophagy and this has been correlated with its beneficial effect on cell and animal models of PolyQ toxicity.

Regarding previous findings about whether GSK-3 activity changes in response to mhtt expression, an increase in the N-terminal phosphorylated form of GSK-3 was first reported in the $STHdh^{Q111/Q111}$ striatal cells (50). Since N-terminal phosphorylation of GSK-3 renders it inactive in some functional scenarios, this was suggestive of reduced GSK-3 activity. Similar increase in p-GSK-3 was also reported in the striatum of R6/1 (28) and more recently also in cortex of R6/1 mice (29) and in R6/2 mice (30), although not in KI140 mice (30). However, no direct analysis of GSK-3 activity had been performed before and only correlation with the level of phosphorylated substrates has been described. Unfortunately, the latter does not provide a clear readout of the kinase activity due to the reported dysregulation in HD of calcineurin (PP2B) (28,30,51,52) and other phosphatases like PHLPP1 (28) or the other major ones PP1 and PP2A (30). The latter might also play a prominent role in regulating N-terminal phosphorylation of GSK-3 as it is decreased in R6/2 mice which show increased N-terminal phosphorylation of GSK-3 while it is not altered in KI140 mice which do not recapitulate the increase in N-terminal phosphorylation of GSK-3 (30). In summary, the here reported decrease in total GSK-3 levels, increased p-GSK-3 in its inhibitory epitopes and decreased enzymatic activity is the first solid demonstration of decreased GSK-3 activity in the brain of a mouse model of HD.

Until very recently, there were no reports on the status of GSK-3 in HD patients. As mentioned, the analysis of p-Ser-GSK-3 is hampered by the instability of the epitope and variability with postmortem interval (33) and only total GSK-3 levels had been explored in cortex and cerebellum but not in the striatum, the most affected brain region (29). Accordingly, the here reported analysis in total GSK-3 levels and enzymatic activity settles that GSK-3 activity is indeed decreased in striatum of HD postmortem brain.

In view of these results, GSK-3-related therapies for HD should not be based on GSK-3 inhibition as initially assumed but on increasing GSK-3 activity. Since no direct activators of GSK-3 are available, such activation could be achieved indirectly by inhibiting kinases such as Akt that are able to phosphorylate GSK-3 at its inhibitory N-terminal serine residue. In fact, Akt inhibitors are close to clinic for cancer (53). Interestingly, the

non-steroid anti-inflammatory drug celecoxib initially developed as a selective inhibitor of COX-2 is known to also inhibit Akt and this is believed to contribute to its anti-cancer effect (54) and 2,5-dymethyl-elecoxib, a derivative that does not inhibit COX-2 has been shown therapeutically useful in cancer and in mouse models of cardiac hypertrophy by inhibiting Akt and thereby activating GSK-3 (55).

Another angle for therapeutic implications of this work would be the identification of the mechanism that mediates between the decrease of GSK-3 activity in HD and the phenotype associated with the disease. As it has been described, dominant-negative GSK-3 transgenic mice develop apoptosis and motor deficits showing an HD-like phenotype (31). It is known that this is mediated by an increase of the FasL/Fas signaling pathway (32,56). Accordingly, reduction of FasL signaling might be a way to counteract the harmful consequences of decreased GSK-3 activity in HD. Another GSK-3-associated mechanism might relate to the efficacy of the transport along microtubules. The latter is responsible for recruitment of toxic monomeric or oligomeric mutant proteins into inert inclusion bodies (57). On the other hand, it has been recently reported an excess of tau in brain of HD patients and mouse models (58) and excess tau results is a less efficient transport along microtubules (59) that can be rescued by increasing GSK-3 activity (60). This might be the reason why the size of mhtt inclusions increases in R6/1 mice with transgenic overexpression of GSK-3. Since this can be protective, pharmacological interventions able to ease transport along microtubules might also be beneficial.

In summary, here we demonstrate that GSK-3 levels and activity are decreased in the striatum of HD patients as well as in other affected brain areas. This is mimicked in the R6/1 mouse model of HD and a moderate increase of GSK-3 in forebrain by genetic manipulation resulted in attenuation of the HD related symptoms of the R6/1 mice thus demonstrating that decreased GSK-3 contributes to HD pathogenesis and offering a new avenue for therapeutic intervention based on approaches that either increase GSK-3 activity or attenuate the effects secondary to the observed GSK-3 decrease.

Materials and Methods

Human brain tissue samples

Brain specimens used in this study from frontal cortex, striatum and hippocampus of HD subjects and controls were provided by Institute of Neuropathology (HUB-ICO-IDIBELL) Brain Bank (Hospitalet de LLobregat, Spain), the Neurological Tissue Bank of the IDIBAPS Biobank (Barcelona, Spain), the Banco de Tejidos Fundación Cien (BT-CIEN, Madrid, Spain) and the Netherlands Brain Bank (Amsterdam, The Netherlands). Written informed consent for brain removal after death for diagnostic and research purposes was obtained from brain donors and/or next of kin. Procedures, information and consent forms have been approved by the Bioethics Subcommittee of Centro Superior de Investigaciones Científicas (Madrid, Spain). The postmortem delay in tissue processing was between 1:00 and 23:30 h (Table 1). The neuropathological examination in HD cases revealed a diagnosis of HD grade from 0-1 to 4 following the criteria of Vonsattel (61).

Table 1. Case information for HD and control cases and experiments for which they have been used

Diagnosis	Vonsattel grade	Sex	Age (years)	PMI	Experiment
HD	3	M	68	4:00	3
HD	n/a	F	28	4:15	1, 2, 3
HD	4	F	64	5:00	1
HD	1	M	59	5:05	1
HD	3	M	59	5:30	1, 3
HD	2/3	F	50	5:40	1
HD	3	M	49	5:45	1
HD	3	F	75	6:00	2, 3
HD	2	M	76	6:00	1
HD	2	M	68	6:10	1
HD	3/4	M	55	7:00	3
HD	3	M	53	7:00	3
HD	n/a	M	62	7:00	2, 3
HD	3	F	72	7:00	3
HD	1	M	73	7:00	1
HD	2	M	71	10:15	1, 3
HD	n/a	F	47	12:00	2, 3
HD	3	M	60	13:05	1, 2, 3
HD	2	M	72	13:10	1
HD	3	F	65	15:15	1, 3
HD	3	F	72	17:00	1, 3
HD	n/a	M	44	n/a	2, 3
HD	n/a	F	69	n/a	2, 3
HD	n/a	F	ND	n/a	2, 3
Control	–	F	57	1:00	2, 3
Control	–	M	78	2:15	1, 3
Control	–	F	78	3:40	1, 3
Control	–	M	56	3:45	1, 2, 3
Control	–	F	81	4:00	2, 3
Control	–	F	64	5:00	1, 3
Control	–	M	85	5:45	1, 3
Control	–	F	70	6:15	1
Control	–	M	76	6:45	1
Control	–	M	55	7:30	1
Control	–	M	51	7:45	1
Control	–	M	68	8:00	2, 3
Control	–	M	60	8:10	1, 3
Control	–	F	71	8:30	1, 3
Control	–	M	71	12:00	1, 3
Control	–	F	60	15:30	1, 2, 3
Control	–	M	31	17:30	1, 2, 3
Control	–	M	79	19:00	2, 3
Control	–	F	81	23:30	1, 3
Control	–	M	56	n/a	2, 3
Control	–	F	58	n/a	2, 3

n/a, not available.
1: western blot; 2: qRT-PCR; 3: GSK-3 activity assay. M, male; F, female; PMI, postmortem interval (h).

Animals

R6/1 mice transgenic for the human exon-1-Htt gene in B6CBAF1 background (62) and GSK-3 overexpression transgenic mice in the B6 background previously generated (34) were used. All mice were housed at the Centro de Biología Molecular "Severo Ochoa" animal facility. Mice were housed four per cage with food and water available *ad libitum* and maintained in a temperature-controlled environment on a 12/12 h light–dark cycle with light onset at 07:00 h. Animal housing and maintenance protocols followed the guidelines of Council of Europe Convention ETS123, recently revised as indicated in the Directive 86/609/EEC. Animal experiments were performed under protocols (P15/P16/P18/P22) approved by the Centro de Biología Molecular Severo Ochoa Institutional Animal Care and Utilization Committee (Comité de Ética de Experimentación Animal del CBM, CEEA-CBM), Madrid, Spain.

Western blot

The samples from different human brain regions that were stored at −80°C were ground with a mortar in a frozen environment with liquid nitrogen to prevent thawing of the samples. The resulting powder was homogenized. For mouse, brains were quickly dissected on an ice-cold plate. Both extracts were prepared by homogenizing the brain areas in ice-cold extraction buffer consisting of 20 mM HEPES, pH 7.4, 100 mM NaCl, 20 mM NaF, 1% Triton X-100, 1 mM sodium orthovanadate, 1 μM okadaic acid, 5 mM sodium pyrophosphate, 30 mM β-glycerophosphate, 5 mM EDTA and protease inhibitors (2 mM PMSF, 10 μg/ml aprotinin, 10 μg/ml leupeptin and 10 μg/ml pepstatin). Samples were homogenized and centrifuged at 15 000 × *g* for 15 min at 4°C. The resulting supernatant was collected, and protein content determined by Bradford assay. Fifteen micrograms of total protein were electrophoresed on 10% SDS–PAGE and transferred to a nitrocellulose membrane and blocked in TBS-T (150 mM NaCl, 20 mM Tris–HCl, pH 7.5, 0.05% Tween 20) supplemented with 5% non-fat dry milk or 5% BSA depending on the antibody used. Employed antibodies are: anti-Gsk-3α/β 1 : 1000 (44–610 form Invitrogen), anti-p-Ser-Gsk-3α/β 1 : 1000 (9331 from Cell Signaling), anti-p-Tyr-GSK-3α/β 1 : 1000 (44604G from Life Technologies) and anti-β-actin (2228 from Sigma). The membranes were incubated with the primary antibody overnight at 4°C in TBS-T supplemented with 5% non-fat dried milk or 5% BSA, washed in TBS-T and next incubated with secondary HRP-conjugated anti-mouse IgG (P0447 from DAKO Cytomation) on anti-rabbit IgG (P0448 from DAKO Cytomation) and developed using the ECL detection kit (Perkin Elmer).

Quantitative real-time reverse transcriptase-PCR

Total tissue RNA was extracted from striatum and cortex of HD and control subjects and from cortex, striatum and hippocampus of R6/1 and WT mice using the Maxwell® 16 LEV simplyRNA Tissue Kit (Promega). The resulting total RNA (750 ng) was used for cDNA synthesis with a Super Script III First-Strand Synthesis SuperMix kit from Invitrogene (PN 11752250) with the amplification protocol 30″ at 95°C + (5″ at 95°C + 5″ at 60°C) × 40 + (5″ at 60°C + 5″ at 95°C). Quantification was performed by real-time PCR using a CFX 384 System (Bio-Rad) in combination with SsoFast Eva Green (Bio-Rad), as per manufacturer's protocol and 1 μl of primer pair was used. Data were analyzed by GenEx 5.3.7 software (Multid AnaLyses AB). The mRNA levels were normalized first relative to total RNA and then relative to the 18S ribosome subunit for human and the mean of 18S ribosome subunit, GADPH, β-actin and β-tubulin gene expression for mouse in each sample. The PCR primers used for human were GSK-3α forward: 5′GTCTCCTACATCTGTTCTCGCTA 3′, GSK-3α reverse: 5′ CAGCCAGCTGACCAAACAT 3′; GSK-3β forward: 5′ GAAAGTATTG CAGGACAAGAGAT 3′; GSK-3β reverse: 5′ CGGACTATGTTACAG TGATCTAG 3′. The PCR primers used for mouse were GSK-3α forward: 5′ GAGCCACAGATTACACCTCGT 3′, GSK-3α reverse: 5′ CTGGCCGAGAAGTAGCTCAG 3′; GSK-3β forward: 5′ GGCAGCAA GGTAACCACAGT 3′ and GSK-3β reverse: 5′ GATGGCAACCAGT TCTCCAG 3′. Transgenic GSK-3β forward: (TGCCACCGAGATATC AAACC), transgenic GSK-3β reverse: (TCGCACAGCTTGAGTAC AGC), total GSK-3β (that detects endogenous and transgenic GSK-3) forward: (ATAAAGATGGCAGCAAGG) and total GSK-3β reverse: (ACCACACCAAATGATCC).

Gsk-3 activity assay

Tissue was homogenized in 20 mM HEPES, pH 7.4, 100 mM NaCl, 10 mM NaF, 1 mM VO_4Na, 1% Triton X-100, 1 mM EDTA, 1 mM EGTA supplemented with a cocktail of protease inhibitors (Roche). Supernatants were collected after centrifugation at 14 000 × *g* for 15 min. The GS1 peptide (YRRAAVPPSPSLSRHSSPHQ-S*EDEE) with phosphorylated ser21 was used as substrate (63). Supernatants were incubated at 37°C with GS1 peptide and [γ-^{32}P] ATP in 25 mM Tris–HCl, pH 7.5, 1 mM DTT, 10 mM $MgCl_2$ and either 10% DMSO or 100 μM mM AR-A014418 (selective GSK-3 inhibitor). The assays were stopped by spotting aliquots on P81 phosphocellulose as described (36). GSK-3 activity was calculated as the difference between the activity in the presence of DMSO and the activity in the presence of AR-A014418.

Immunohistochemistry and immunofluorescence

Mice were sacrificed using CO_2 and brains immediately removed and dissected on an ice-cold plate. Left hemispheres were processed for histology placed in 4% paraformaldehyde in Sorensen's phosphate buffer (PFA) overnight, and then immersed in 30% sucrose in PBS for 72 h. Once cryoprotected, the samples were included in OCT compound (Sakura Finetek Europe), frozen and stored at −80°C until use. 30 μm sagittal sections were cut on a cryostat (Thermo Scientific) and collected and stored free floating in glycol containing buffer (30% glycerol, 30% ethylene glycol in 0.02 M phosphate buffer) at −20°C. Subsequently, sections were immersed in 0.3% H_2O_2 in PBS for 30 min to quench endogenous peroxidase activity. For immunohistochemical staining, sections were blocked for 1 h in PBS containing 0.5% fetal bovine serum, 0.3% Triton X-100 and 1% BSA (Sigma-Aldrich). Sections were incubated overnight at 4°C in PBS containing 0.3% Triton X-100 and 1% BSA with the corresponding primary antibodies: anti-β-galactosidase 1 : 2000 (0855976 from MD Biomedicals) and anti-Huntingtin clone EM48 1 : 100 (MAB5374 from Millipore), anti-DARPP32 1 : 1000 (611520 from BD Bioscience) and anti-p-Ser-GSK-3α/β 1 : 200 (9331 from Cell Signaling). Finally, brain sections were incubated in avidin–biotin complex using the Elite Vectastain kit (Vector Laboratories). Chromogen reactions were performed with diaminobenzidine (SIGMAFAST™ DAB, Sigma) for 10 min. Sections were mounted on glass slides and coverslipped with Mowiol (Calbiochem). Images were captured using an Olympus BX41 microscope with an Olympus camera DP-70 (Olympus Denmark A/S). For immunofluorescence, sections were pretreated with 0.1% Triton X-100 for 15 min, 1 M glycine for 30 min and blocking solution (1% BSA and 0.1% Triton X-100) for 1 h. Sections were then incubated overnight at 4°C with the following primary antibodies in blocking solution: anti-Gsk-3β 1 : 500 (9315 from Cell Signaling), anti-β-galactosidase 1 : 2000 (z3781 from Promega), anti-p-Ser-GSK-3α/β 1 : 200 (9331 from Cell Signaling), anti-NeuN 1 : 1000 (MAB377 from Millipore) and anti-GFAP 1 : 500 (60331D from Pharmingen). The following day, sections were washed in PBS. Then sections were incubated in avidin–biotin complex using the Elite Vectastain kit (Vector Laboratories) for 1 h and after that, sections were incubated with goat anti-rabbit Alexa 488 (Invitrogen) and goat anti-mouse Alexa 555 (Invitrogen) secondary antibodies for 1 h. Nuclei were counterstained with DAPI (Calbiochem). Images were acquired with a laser confocal LSM710 system coupled to the invert Axioobserver microscope with a ×63, 1.4 numerical aperture oil immersion objective using the Zen2010B sp1 software (Carl Zeiss). Images were processed using ImageJ 1.45 s.

Stereological quantification of brain volume and huntingtin aggregates

Diaminobenzidine immunohistochemistry was performed as previously described (64). Tissue was incubated with the primary

antibodies anti-DARPP32 1 : 1000 (611520 from BD Bioscience) or anti-EM48 1 : 100 (MAB5374 from Millipore), followed by the corresponding biotinylated secondary antibody 1 : 200 (Thermo Fisher). For estimation of cortical, striatal and hippocampal volumes, 12 sagittal sections per animal spaced 240 μm apart were examined. Unbiased blinded to genotype counting was performed with Computer-Assisted Stereology Toolbox (CAST) software (Olympus Danmark A/S, Ballerup, Denmark). Automated quantification of the number and size of huntingtin aggregates within the striatum was performed using CellProfiler v2.8 software. Briefly, five sagittal striatal sections per animal spaced 240 μm apart were chosen for the analysis. Images from the 100% of the striatum were acquired at ×20 magnification and EM48 staining was used to identify nuclear inclusions and delimitate their area. The CellProfiler pipeline file containing the specific parameters of the automated quantification is available upon request.

Behavioral testing

Open field test

Locomotor activity was measured at the age of 4.5 months in clear plexiglas boxes measuring 43.2× 43.2 cm, outfitted with photobeam detectors for monitoring horizontal and vertical activity. Activity levels were recorded with an MED Associates' Activity Monitor (MED Associates, St. Albans, VT, USA). Locomotor activity data were collected via a PC and was analyzed with the MED Associates' Activity Monitor Data Analysis software. Mice were placed in a corner of the open-field apparatus and left to move freely. Variables recorded included ambulatory distance (cm) and vertical counts. Data were individually recorded for each animal during 15 min. The number of animals used for this test was WT, $n = 19$ (males $n = 8$, females $n = 11$); LowTgGsk-3, $n = 22$ (males $n = 10$, females $n = 12$); HighTgGsk-3, $n = 13$ (males $n = 3$, females $n = 10$); R6/1, $n = 19$ (males $n = 6$, females $n = 13$); R6/1 + LowTgGsk-3, $n = 17$ (males $n = 8$, females $n = 9$); R6/1 + HighTgGsk-3, $n = 7$ (males $n = 2$, females $n = 5$).

Rotarod test

Rotarod test was performed at the age of 2, 4, 6 and 8 months with accelerating rotarod apparatus (Ugo Basile). Mice were pretrained during two days at a constant speed, 4 rpm the first day over 1 min four times or 8 rpm over 1 min four times the second day. On the third day, rotarod was set to accelerate from 4 to 40 rpm over 5 min and mice were tested four times. During accelerating trials, the latency to fall from the rod was measured. The number of animals used for this test was: R6/1, $n = 35$ (males $n = 11$, females $n = 24$); R6/1 + LowTgGsk-3, $n = 26$ (males $n = 12$, females $n = 14$); R6/1 + HighTgGsk-3, $n = 12$ (males $n = 6$, females $n = 6$).

Contextual fear conditioning test

The test was performed at the age of 5 months using the Startfear 1.06 system for fear conditioning from Panlab. During training, mice stayed in the conditioning chamber for a total of 6 min 30 s. After 2 min of exploration, an 85 dB sound was emitted for 30 s and a 0.2 mA foot-shock was superposed to the tone during the last 2 s (three times). Thirty seconds after the last foot-shock, the mouse was removed from the chamber and returned to its home cage. Twenty-four hours after the conditioning session, the contextual memory was assessed by introducing the mouse in the conditioning chamber. The behavioral index use to quantify the memory of context conditioning is freezing, a species-specific tonic immobility response. Freezing is defined as a tonic immobilization, with total absence of movement except those due to breathing. Freezing scores were assessed during 6 min, no tone or foot-shock being presented to the animal during this test. The number of animals used for this test was: WT, $n = 32$ (males $n = 5$, females $n = 27$); LowTgGsk-3, $n = 32$ (males $n = 19$, females $n = 13$); HighTgGsk-3, $n = 22$ (males $n = 5$, females $n = 17$); R6/1, $n = 27$ (males $n = 8$, females $n = 19$); R6/1 + LowTgGsk-3, $n = 26$ (males $n = 12$, females $n = 14$); R6/1 + HighTgGsk-3, $n = 10$ (males $n = 6$, females $n = 4$).

Data analysis

Statistical analysis was performed with SPSS 19.0 (SPSS® Statistic IBM®). Data are represented as means ± SEM. The normality of the data was analyzed by Shapiro-Wilk test. For two-group comparison, two tail Student's *t*-test (data with normal distribution) or Mann–Whitney *U*-test (data with non-normal distribution) was performed. For multiple comparisons, data with a normal distribution were analyzed by one-way ANOVA test followed by a DMS or a Games–Howell *post hoc* test. Statistical significance of non-parametric data was determined by Kruskal–Wallis test when analyzing all experimental groups followed by a Mann–Whitney *U*-test for analysis of paired genotypes. A critical value for significance of $P < 0.05$ was used throughout the study.

Supplementary Material

Supplementary Material is available at *HMG* online.

Acknowledgements

We thank Dr Alberto Rábano from Banco de Tejidos Fundación Cien (BT-CIEN, Madrid) for advice on human sample analysis. We also thank Miriam Lucas and the CBMSO Genomics Facility for their excellent technical assistance and members of the Lucas' Lab for helpful advice and critical reading of the manuscript.

Conflict of Interest statement. None declared.

Funding

This work was supported by Centro de Investigación Biomédica en Red de Enfermedades Neurodegenerativas (CiberNed-Instituto de salud Carlos III) and by grants from Ministerio de Ciencia (MEC, MICINN, MINECO), Comunidad Autónoma de Madrid and Fundación Ramón Areces. M.F.-N. was recipient of a CSIC JAE-pre research contract.

References

1. Vonsattel, J.P. and DiFiglia, M. (1998) Huntington disease. *J Neuropathol Exp Neurol*, **57**, 369–384.
2. HDCRG. (1993) A novel gene containing a trinucleotide repeat that is expanded and unstable on Huntington's disease chromosomes. The Huntington's Disease Collaborative Research Group. *Cell*, **72**, 971–983.
3. Ross, C.A. and Tabrizi, S.J. (2011) Huntington's disease: from molecular pathogenesis to clinical treatment. *Lancet Neurol*, **10**, 83–98.
4. Woodgett, J.R. (1990) Molecular cloning and expression of glycogen synthase kinase-3/factor A. *EMBO J*, **9**, 2431–2438.

5. Beurel, E., Grieco, S.F. and Jope, R.S. (2014) Glycogen synthase kinase-3 (GSK3): regulation, actions, and diseases. *Pharmacol Ther*.
6. Grimes, C.A. and Jope, R.S. (2001) The multifaceted roles of glycogen synthase kinase 3beta in cellular signaling. *Prog Neurobiol*, **65**, 391–426.
7. Doble, B.W. and Woodgett, J.R. (2003) GSK-3: tricks of the trade for a multi-tasking kinase. *J Cell Sci*, **116**, 1175–1186.
8. Beaulieu, J.M., Marion, S., Rodriguiz, R.M., Medvedev, I.O., Sotnikova, T.D., Ghisi, V., Wetsel, W.C., Lefkowitz, R.J., Gainetdinov, R.R. and Caron, M.G. (2008) A beta-arrestin 2 signaling complex mediates lithium action on behavior. *Cell*, **132**, 125–136.
9. O'Brien, W.T., Huang, J., Buccafusca, R., Garskof, J., Valvezan, A.J., Berry, G.T. and Klein, P.S. (2011) Glycogen synthase kinase-3 is essential for beta-arrestin-2 complex formation and lithium-sensitive behaviors in mice. *J Clin Invest*, **121**, 3756–3762.
10. Su, P., Li, S., Chen, S., Lipina, T.V., Wang, M., Lai, T.K., Lee, F.H., Zhang, H., Zhai, D., Ferguson, S.S. *et al.* (2014) A dopamine D2 receptor-DISC1 protein complex may contribute to antipsychotic-like effects. *Neuron*, **84**, 1302–1316.
11. Hernandez, F., Lucas, J.J. and Avila, J. (2013) GSK3 and tau: two convergence points in Alzheimer's disease. *J Alzheimers Dis*, 33(Suppl. 1), S141–S144.
12. Beaulieu, J.M., Sotnikova, T.D., Yao, W.D., Kockeritz, L., Woodgett, J.R., Gainetdinov, R.R. and Caron, M.G. (2004) Lithium antagonizes dopamine-dependent behaviors mediated by an AKT/glycogen synthase kinase 3 signaling cascade. *Proc Natl Acad Sci USA*, **101**, 5099–5104.
13. Li, X., Liu, M., Cai, Z. and Wang, G. (2010) Regulation of glycogen synthase kinase-3 during bipolar mania treatment. *Bipolar Disord*, **12**, 741–752.
14. Grof, P. and Muller-Oerlinghausen, B. (2009) A critical appraisal of lithium's efficacy and effectiveness: the last 60 years. *Bipolar Disord*, **11**(Suppl. 2), 10–19.
15. Macdonald, A., Briggs, K., Poppe, M., Higgins, A., Velayudhan, L. and Lovestone, S. (2008) A feasibility and tolerability study of lithium in Alzheimer's disease. *Int J Geriatr Psychiatry*, **23**, 704–711.
16. Forlenza, O.V., Diniz, B.S., Radanovic, M., Santos, F.S., Talib, L. L. and Gattaz, W.F. (2011) Disease-modifying properties of long-term lithium treatment for amnestic mild cognitive impairment: randomised controlled trial. *Br J Psychiatry*, **198**, 351–356.
17. Cohen, P. and Goedert, M. (2004) GSK3 inhibitors: development and therapeutic potential. *Nat Rev Drug Discov*, **3**, 479–487.
18. Arfeen, M. and Bharatam, P.V. (2013) Design of glycogen synthase kinase-3 inhibitors: an overview on recent advancements. *Curr Pharm Des*, **19**, 4755–4775.
19. Lovestone, S., Boada, M., Dubois, B., Hull, M., Rinne, J.O., Huppertz, H., Calero, M., Andres, M.V., Gomez-Carrillo, B., Leon, T. *et al.* (2014) A Phase II trial of Tideglusib in Alzheimer's disease. *J Alzheimers Dis*.
20. Carmichael, J., Sugars, K.L., Bao, Y.P. and Rubinsztein, D.C. (2002) Glycogen synthase kinase-3beta inhibitors prevent cellular polyglutamine toxicity caused by the Huntington's disease mutation. *J Biol Chem*, **277**, 33791–33798.
21. Valencia, A., Reeves, P.B., Sapp, E., Li, X., Alexander, J., Kegel, K.B., Chase, K., Aronin, N. and DiFiglia, M. (2010) Mutant huntingtin and glycogen synthase kinase 3-beta accumulate in neuronal lipid rafts of a presymptomatic knock-in mouse model of Huntington's disease. *J Neurosci Res*, **88**, 179–190.
22. Voisine, C., Varma, H., Walker, N., Bates, E.A., Stockwell, B.R. and Hart, A.C. (2007) Identification of potential therapeutic drugs for Huntington's disease using Caenorhabditis elegans. *PLoS One*, **2**, e504.
23. Berger, Z., Ttofi, E.K., Michel, C.H., Pasco, M.Y., Tenant, S., Rubinsztein, D.C. and O'Kane, C.J. (2005) Lithium rescues toxicity of aggregate-prone proteins in Drosophila by perturbing Wnt pathway. *Hum Mol Genet*, **14**, 3003–3011.
24. Wood, N.I. and Morton, A.J. (2003) Chronic lithium chloride treatment has variable effects on motor behaviour and survival of mice transgenic for the Huntington's disease mutation. *Brain Res Bull*, **61**, 375–383.
25. Chiu, C.T., Liu, G., Leeds, P. and Chuang, D.M. (2011) Combined treatment with the mood stabilizers lithium and valproate produces multiple beneficial effects in transgenic mouse models of Huntington's disease. *Neuropsychopharmacology*, **36**, 2406–2421.
26. Scheuing, L., Chiu, C.T., Liao, H.M., Linares, G.R. and Chuang, D.M. (2014) Preclinical and clinical investigations of mood stabilizers for Huntington's disease: what have we learned? *Int J Biol Sci*, **10**, 1024–1038.
27. Sarkar, S., Krishna, G., Imarisio, S., Saiki, S., O'Kane, C.J. and Rubinsztein, D.C. (2008) A rational mechanism for combination treatment of Huntington's disease using lithium and rapamycin. *Hum Mol Genet*, **17**, 170–178.
28. Saavedra, A., Garcia-Martinez, J.M., Xifro, X., Giralt, A., Torres-Peraza, J.F., Canals, J.M., Diaz-Hernandez, M., Lucas, J.J., Alberch, J. and Perez-Navarro, E. (2010) PH domain leucine-rich repeat protein phosphatase 1 contributes to maintain the activation of the PI3K/Akt pro-survival pathway in Huntington's disease striatum. *Cell Death Differ*, **17**, 324–335.
29. Lim, N.K., Hung, L.W., Pang, T.Y., McLean, C.A., Liddell, J.R., Hilton, J.B., Li, Q.X., White, A.R., Hannan, A.J. and Crouch, P. J. (2014) Localized changes to glycogen synthase kinase-3 and collapsin response mediator protein-2 in the Huntington's disease affected brain. *Hum Mol Genet*, **23**, 4051–4063.
30. Blum, D., Herrera, F., Francelle, L., Mendes, T., Basquin, M., Obriot, H., Demeyer, D., Sergeant, N., Gerhardt, E., Brouillet, E. *et al.* (2014) Mutant huntingtin alters Tau phosphorylation and subcellular distribution. *Hum Mol Genet*.
31. Gomez-Sintes, R., Hernandez, F., Bortolozzi, A., Artigas, F., Avila, J., Zaratin, P., Gotteland, J.P. and Lucas, J.J. (2007) Neuronal apoptosis and reversible motor deficit in dominant-negative GSK-3 conditional transgenic mice. *EMBO J*, **26**, 2743–2754.
32. Gomez-Sintes, R. and Lucas, J.J. (2013) Neuronal apoptosis and motor deficits in mice with genetic inhibition of GSK-3 are Fas-dependent. *PLoS ONE*, **8**, e70952.
33. Li, X., Friedman, A.B., Roh, M.S. and Jope, R.S. (2005) Anesthesia and post-mortem interval profoundly influence the regulatory serine phosphorylation of glycogen synthase kinase-3 in mouse brain. *J Neurochem*, **92**, 701–704.
34. Lucas, J.J., Hernandez, F., Gomez-Ramos, P., Moran, M.A., Hen, R. and Avila, J. (2001) Decreased nuclear beta-catenin, tau hyperphosphorylation and neurodegeneration in GSK-3beta conditional transgenic mice. *EMBO J*, **20**, 27–39.
35. Hernandez, F., Borrell, J., Guaza, C., Avila, J. and Lucas, J.J. (2002) Spatial learning deficit in transgenic mice that conditionally over-express GSK-3beta in the brain but do not form tau filaments. *J Neurochem*, **83**, 1529–1533.
36. Engel, T., Hernandez, F., Avila, J. and Lucas, J.J. (2006) Full reversal of Alzheimer's disease-like phenotype in a mouse model with conditional overexpression of glycogen synthase kinase-3. *J Neurosci*, **26**, 5083–5090.

37. Beurel, E. and Jope, R.S. (2006) The paradoxical pro- and anti-apoptotic actions of GSK3 in the intrinsic and extrinsic apoptosis signaling pathways. *Prog Neurobiol*, **79**, 173–189.
38. Hooper, C., Killick, R. and Lovestone, S. (2008) The GSK3 hypothesis of Alzheimer's disease. *J Neurochem*, **104**, 1433–1439.
39. Leroy, K., Yilmaz, Z. and Brion, J.P. (2007) Increased level of active GSK-3beta in Alzheimer's disease and accumulation in argyrophilic grains and in neurones at different stages of neurofibrillary degeneration. *Neuropathol Appl Neurobiol*, **33**, 43–55.
40. Hye, A., Kerr, F., Archer, N., Foy, C., Poppe, M., Brown, R., Hamilton, G., Powell, J., Anderton, B. and Lovestone, S. (2005) Glycogen synthase kinase-3 is increased in white cells early in Alzheimer's disease. *Neurosci Lett*, **373**, 1–4.
41. Pei, J.J., Tanaka, T., Tung, Y.C., Braak, E., Iqbal, K. and Grundke-Iqbal, I. (1997) Distribution, levels, and activity of glycogen synthase kinase-3 in the Alzheimer disease brain. *J Neuropathol Exp Neurol*, **56**, 70–78.
42. Imahori, K. and Uchida, T. (1997) Physiology and pathology of tau protein kinases in relation to Alzheimer's disease. *J Biochem*, **121**, 179–188.
43. Meijer, L., Flajolet, M. and Greengard, P. (2004) Pharmacological inhibitors of glycogen synthase kinase 3. *Trends Pharmacol Sci*, **25**, 471–480.
44. Noble, W., Planel, E., Zehr, C., Olm, V., Meyerson, J., Suleman, F., Gaynor, K., Wang, L., LaFrancois, J., Feinstein, B. *et al.* (2005) Inhibition of glycogen synthase kinase-3 by lithium correlates with reduced tauopathy and degeneration in vivo. *Proc Natl Acad Sci USA*, **102**, 6990–6995.
45. Engel, T., Goni-Oliver, P., Lucas, J.J., Avila, J. and Hernandez, F. (2006) Chronic lithium administration to FTDP-17 tau and GSK-3beta overexpressing mice prevents tau hyperphosphorylation and neurofibrillary tangle formation, but pre-formed neurofibrillary tangles do not revert. *J Neurochem*, **99**, 1445–1455.
46. Wei, H., Qin, Z.H., Senatorov, V.V., Wei, W., Wang, Y., Qian, Y. and Chuang, D.M. (2001) Lithium suppresses excitotoxicity-induced striatal lesions in a rat model of Huntington's disease. *Neuroscience*, **106**, 603–612.
47. Watase, K., Gatchel, J.R., Sun, Y., Emamian, E., Atkinson, R., Richman, R., Mizusawa, H., Orr, H.T., Shaw, C. and Zoghbi, H.Y. (2007) Lithium therapy improves neurological function and hippocampal dendritic arborization in a spinocerebellar ataxia type 1 mouse model. *PLoS Med*, **4**, e182.
48. Gould, T.D., Picchini, A.M., Einat, H. and Manji, H.K. (2006) Targeting glycogen synthase kinase-3 in the CNS: implications for the development of new treatments for mood disorders. *Curr Drug Targets*, **7**, 1399–1409.
49. Xu, W., Li, Z., Yu, B., He, X., Shi, J., Zhou, R., Liu, D. and Wu, Z. (2013) Effects of DNMT1 and HDAC inhibitors on gene-specific methylation reprogramming during porcine somatic cell nuclear transfer. *PLoS ONE*, **8**, e64705.
50. Gines, S., Ivanova, E., Seong, I.S., Saura, C.A. and MacDonald, M.E. (2003) Enhanced Akt signaling is an early pro-survival response that reflects N-methyl-D-aspartate receptor activation in Huntington's disease knock-in striatal cells. *J Biol Chem*, **278**, 50514–50522.
51. Xifro, X., Giralt, A., Saavedra, A., Garcia-Martinez, J.M., Diaz-Hernandez, M., Lucas, J.J., Alberch, J. and Perez-Navarro, E. (2009) Reduced calcineurin protein levels and activity in exon-1 mouse models of Huntington's disease: role in excitotoxicity. *Neurobiol Dis*, **36**, 461–469.
52. Gratuze, M., Noel, A., Julien, C., Cisbani, G., Milot-Rousseau, P., Morin, F., Dickler, M., Goupil, C., Bezeau, F., Poitras, I. *et al.* (2014) Tau hyperphosphorylation and deregulation of calcineurin in mouse models of Huntington's disease. *Hum Mol Genet*.
53. Hong, D.S., Henary, H., Falchook, G.S., Naing, A., Fu, S., Moulder, S., Wheler, J.J., Tsimberidou, A., Durand, J.B., Khan, R. *et al.* (2014) First-in-human study of pbi-05204, an oleander-derived inhibitor of akt, fgf-2, nf-kappaBeta and p70s6k, in patients with advanced solid tumors. *Invest New Drugs*, **32**, 1204–1212.
54. Yang, H.M., Kim, H.S., Park, K.W., You, H.J., Jeon, S.I., Youn, S. W., Kim, S.H., Oh, B.H., Lee, M.M., Park, Y.B. *et al.* (2004) Celecoxib, a cyclooxygenase-2 inhibitor, reduces neointimal hyperplasia through inhibition of Akt signaling. *Circulation*, **110**, 301–308.
55. Takahashi-Yanaga, F. (2013) Activator or inhibitor? GSK-3 as a new drug target. *Biochem Pharmacol*, **86**, 191–199.
56. Gomez-Sintes, R. and Lucas, J.J. (2010) NFAT/Fas signaling mediates the neuronal apoptosis and motor side effects of GSK-3 inhibition in a mouse model of lithium therapy. *J Clin Invest*, **120**, 2432–2445.
57. Kawaguchi, Y., Kovacs, J.J., McLaurin, A., Vance, J.M., Ito, A. and Yao, T.P. (2003) The deacetylase HDAC6 regulates aggresome formation and cell viability in response to misfolded protein stress. *Cell*, **115**, 727–738.
58. Fernandez-Nogales, M., Cabrera, J.R., Santos-Galindo, M., Hoozemans, J.J., Ferrer, I., Rozemuller, A.J., Hernandez, F., Avila, J. and Lucas, J.J. (2014) Huntington's disease is a four-repeat tauopathy with tau nuclear rods. *Nat Med*, **20**, 881–885.
59. Ebneth, A., Godemann, R., Stamer, K., Illenberger, S., Trinczek, B. and Mandelkow, E. (1998) Overexpression of tau protein inhibits kinesin-dependent trafficking of vesicles, mitochondria, and endoplasmic reticulum: implications for Alzheimer's disease. *J Cell Biol*, **143**, 777–794.
60. Spittaels, K., Van den Haute, C., Van Dorpe, J., Geerts, H., Mercken, M., Bruynseels, K., Lasrado, R., Vandezande, K., Laenen, I., Boon, T. *et al.* (2000) Glycogen synthase kinase-3beta phosphorylates protein tau and rescues the axonopathy in the central nervous system of human four-repeat tau transgenic mice. *J Biol Chem*, **275**, 41340–41349.
61. Vonsattel, J.P., Myers, R.H., Stevens, T.J., Ferrante, R.J., Bird, E. D. and Richardson, E.P. Jr. (1985) Neuropathological classification of Huntington's disease. *J Neuropathol Exp Neurol*, **44**, 559–577.
62. Mangiarini, L., Sathasivam, K., Seller, M., Cozens, B., Harper, A., Hetherington, C., Lawton, M., Trottier, Y., Lehrach, H., Davies, S.W. *et al.* (1996) Exon 1 of the HD gene with an expanded CAG repeat is sufficient to cause a progressive neurological phenotype in transgenic mice. *Cell*, **87**, 493–506.
63. Stambolic, V. and Woodgett, J.R. (1994) Mitogen inactivation of glycogen synthase kinase-3 beta in intact cells via serine 9 phosphorylation. *Biochem J*, **303**(Pt 3), 701–704.
64. Giralt, A., Friedman, H.C., Caneda-Ferron, B., Urban, N., Moreno, E., Rubio, N., Blanco, J., Peterson, A., Canals, J.M. and Alberch, J. (2010) BDNF regulation under GFAP promoter provides engineered astrocytes as a new approach for long-term protection in Huntington's disease. *Gene Ther*, **17**, 1294–1308.

Figure 3.

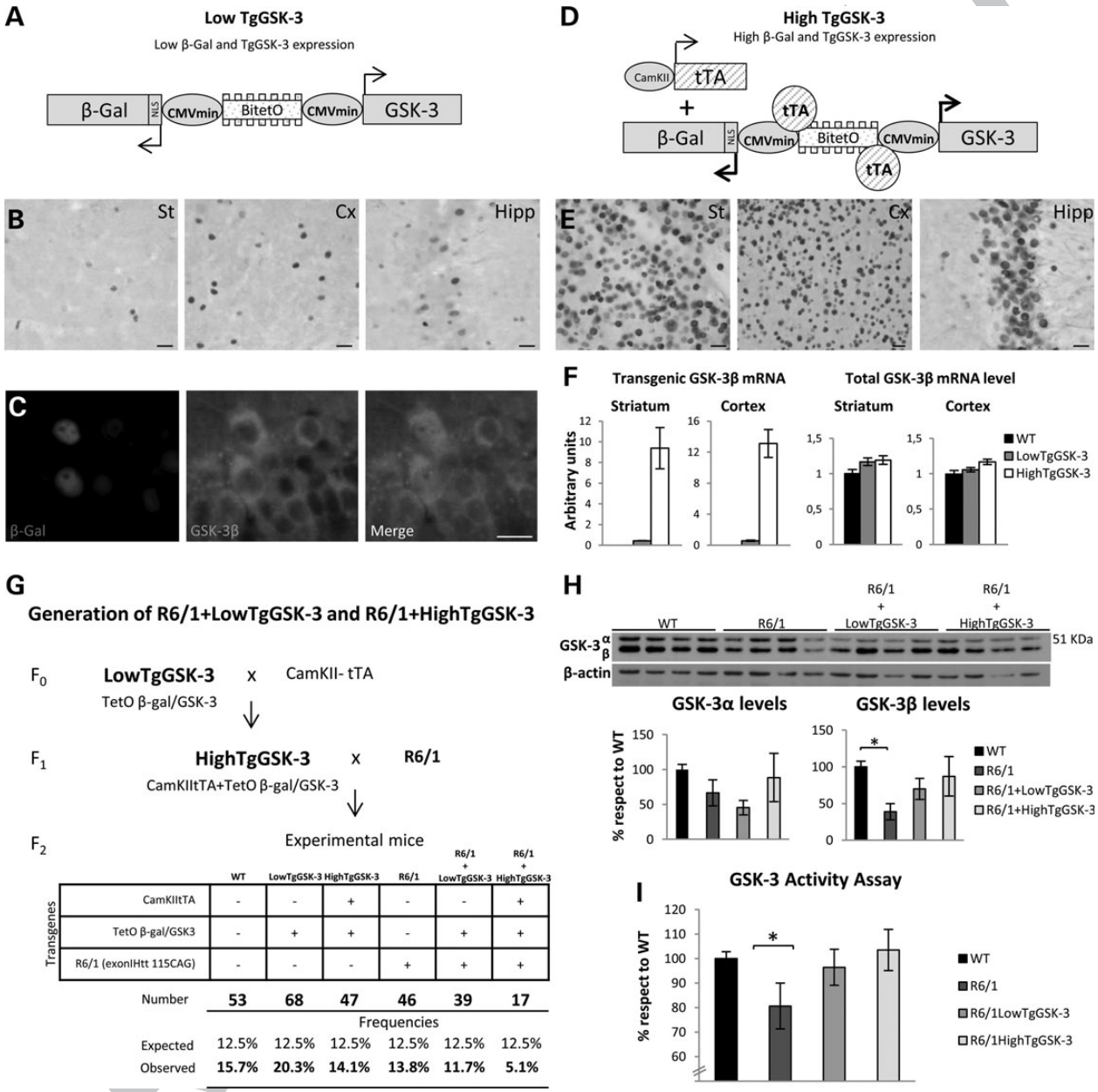

	WT	LowTgGSK-3	HighTgGSK-3	R6/1	R6/1 + LowTgGSK-3	R6/1 + HighTgGSK-3
Transgenes: CamKIItTA	-	-	+	-	-	+
TetO β-gal/GSK3	-	+	+	-	+	+
R6/1 (exonIHtt 115CAG)	-	-	-	+	+	+
Number	53	68	47	46	39	17
Frequencies						
Expected	12.5%	12.5%	12.5%	12.5%	12.5%	12.5%
Observed	**15.7%**	**20.3%**	**14.1%**	**13.8%**	**11.7%**	**5.1%**

Figure 4.

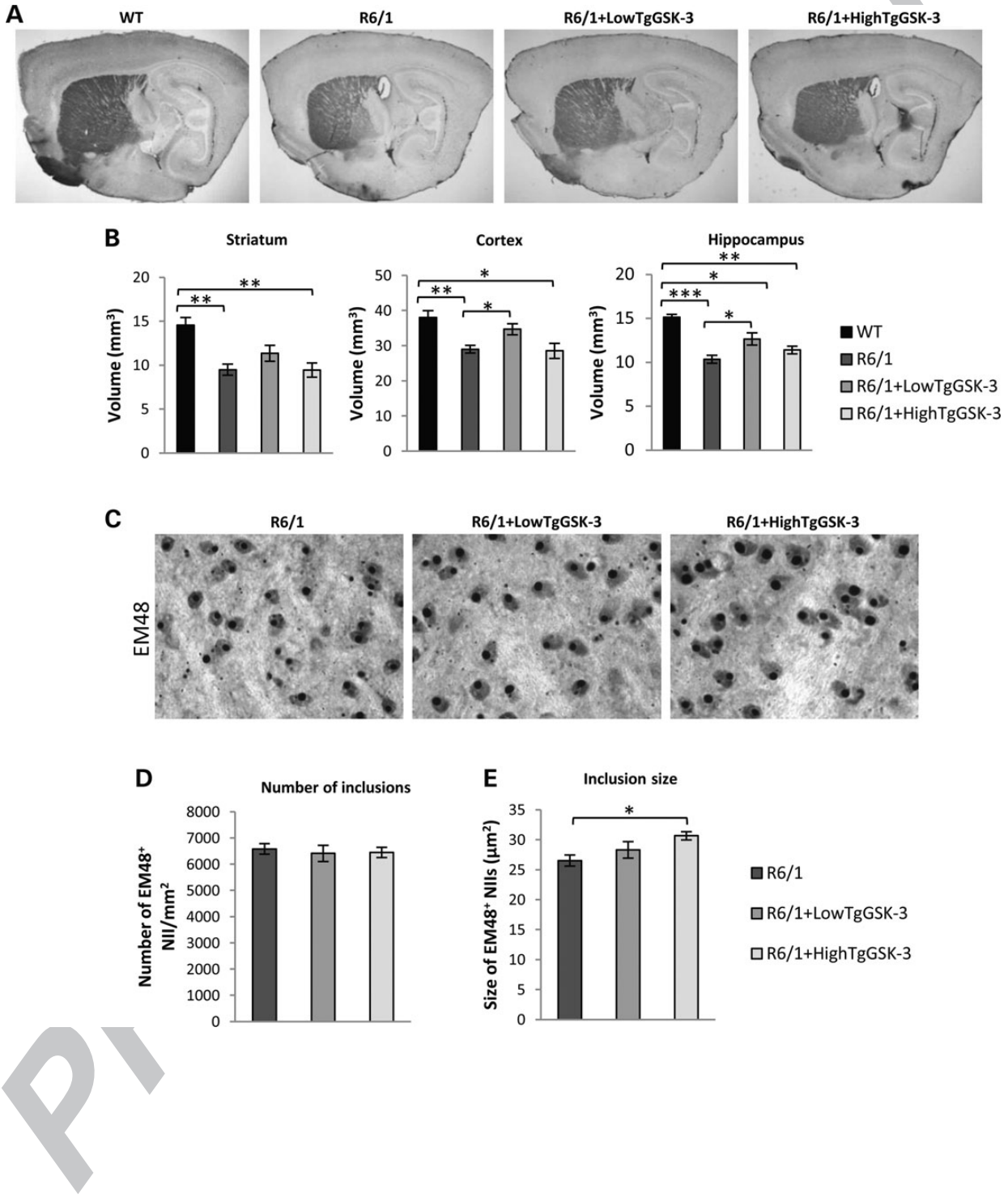
A
WT
R6/1
R6/1+LowTgGSK-3
R6/1+HighTgGSK-3
B
Striatum
Cortex
Hippocampus
Volume (mm³)
WT
R6/1
R6/1+LowTgGSK-3
R6/1+HighTgGSK-3
C
R6/1
R6/1+LowTgGSK-3
R6/1+HighTgGSK-3
EM48
D
Number of inclusions
Number of EM48⁺ NII/mm²
E
Inclusion size
Size of EM48⁺ NIIs (µm²)
R6/1
R6/1+LowTgGSK-3
R6/1+HighTgGSK-3

Figure 5.